Poly-ion complex micelle effectively delivers CoA-conjugated CPT1 inhibitors to modulate lipid metabolism in brain cells

West Kristian D. Paraiso[1], Jesús Garcia-Chica[2,3,4], Xavier Ariza[3,5], Sebastián Zagmutt[2], Shigeto Fukushima[1], Jordi Garcia[3,5], Yuki Mochida[1], Dolors Serra[4,5], Laura Herrero[4,5], Hiroaki Kinoh[1], Núria Casals[2,5], Kazunori Kataoka[1,6], Rosalía Rodríguez-Rodríguez[2,*], and Sabina Quader[1,*]

[1]Innovation Center of Nanomedicine, Kawasaki Institute of Industrial Promotion, Kawasaki, Kanagawa 210-0821 Japan

[2]Basic Sciences Department, Faculty of Medicine and Health Sciences, Universitat Internacional de Catalunya, Sant Cugat del Vallès, E-08195 Spain.

[3]Department of Inorganic and Organic Chemistry, Faculty of Chemistry, Institut de Biomedicina de la Universitat de Barcelona (IBUB), Universitat de Barcelona, Barcelona, E-08028 Spain.

[4]Department of Biochemistry and Physiology, School of Pharmacy and Food Sciences, Institut de Biomedicina de la Universitat de Barcelona (IBUB), Universitat de Barcelona, Barcelona, E-08028 Spain.

[5]Centro de Investigación Biomédica en Red de Fisiopatología de la Obesidad y la Nutrición (CIBEROBN), Instituto de Salud Carlos III, Madrid, E-28029 Spain.

[6]Institute for Future Initiatives, The University of Tokyo, Tokyo 113-0033 Japan.

***Corresponding authors**: Rosalía Rodríguez-Rodríguez (rrodriguez@uic.es) (Tel. +34-935-042-002) and Sabina Quader (sabina-q@kawasaki-net.ne.jp) (Tel. +81-44-589-5920)

ABSTRACT

Carnitine palmitoyltransferase 1 (CPT1) is a central player in lipid metabolism, catalyzing the first committed step to fatty acid oxidation (FAO), and is an appealing target for several diseases. However, CoA-conjugated CPT1 inhibitors are negatively-charged and have low cell membrane permeability. Herein, we report the use of a poly-ion complex (PIC) micelles to deliver the specific CPT1 inhibitors, (±)-, (+)-, and (-)-C75-CoA into U87MG glioma cells and GT1-7 neurons. PIC micelles were formed through charge-neutralization of the cargo with the cationic side chain of PEG-poly{N-[N'-(2-aminoethyl)-2-aminoethyl]aspartamide} (PEG-PAsp(DET)), forming 50-60-nm particles with a neutral surface charge. Upon short-term incubation with cells, the micelle-encapsulated CPT1 inhibitors resulted in 1.5 to 5-fold reduction of ATP synthesis, compared to the free drug, without an apparent decline in cell viability. Micelle treatment showed a discernible decrease in oxidation of ^{14}C-palmitate into CO_2 and acid-soluble FAO metabolites, confirming that the substantial lowering of ATP production was related to FAO inhibition. Micelle treatment also diminished IC_{50} by 2 to 4-fold over the free-drug-treated U87MG after long-term incubation. The resulting IC_{50} is comparable with etomoxir. We synthesized a fluorescent CoA derivative and encapsulated it in the PIC micelle to measure cellular uptake. The fluorescent micelle showed more efficient internalization in both cell types, especially in neurons where uptake reached up to 3-fold over the free dye. The results starkly demonstrate that the PIC micelle is a promising delivery system for anionic inhibitors of CPT1 in glioma cells and neurons, laying the groundwork for future research or clinical applications.

1. INTRODUCTION

Lipids, which include triglycerides, phospholipids, steroids, and other fat-soluble biological molecules, are important elements of the brain's structure and function, where they constitute 50% of its dry weight [1,2]. Among these, fatty acids (FAs) function as energy source, lipid membrane component, as well as starting material for signaling molecules [3]. Carnitine palmitoyltransferase 1 (CPT1) is an enzyme that catalyzes the rate-limiting step in fatty acid oxidation (FAO) – transesterification of LCFA-CoA (long-chain fatty acid-coenzyme A) and carnitine to form CoA and LCFA-carnitine esters. The resulting LCFA-carnitine can then be transported across membranes for further metabolism [4].

The CPT1 system is pivotal for the regulation of FA metabolism in most of the tissues. In the brain, particularly in hypothalamic neurons, CPT1 has been revealed as a potential target against obesity [5]. Accordingly, knockdown and pharmacological inhibition of CPT1 in the hypothalamus contributes to reduced food intake in rodents because of the accumulation of LCFA-CoA in the neurons [6–8]. This is thought to be a satiety signal as it precedes reduced expression of orexigenic (feeding-promoting) proteins, leading to reduced food intake [9,10], making it an appealing target for obesity. In addition to hypothalamic neurons for the regulation of energy homeostasis, CPT1 is crucial to the survival of certain cancer types, including brain cancer. Particularly, glioblastoma (GB) has been related to increased CPT1 expression and FA metabolism alterations. Importantly, this elevated expression of CPT1 is a very common event (90-95% cases) among human diffuse gliomas [11–13]. CPT1-expressing tumor cells show increased FAO, promoting survival in conditions of metabolic stress like glucose deprivation and hypoxia [14]. While tumor molecular heterogeneity is an emerging critical concern in oncology, homogeneous elevated expression of CPT1 in GB is indeed an attractive molecular target for GB therapy.

Several pharmacological inhibitors of CPT1, which act by competing with the natural inhibitor malonyl-CoA, have been investigated [15]. An example is etomoxir (ETO), which is converted to etomoxiryl-CoA and acts on CPT1 *in vivo*, leading to decreased body weight and food intake in rodents [16,17]. However, it was deemed too toxic for clinical use, exemplified by causing severe hepatotoxicity as a side effect [18].

A more promising compound is (±)-C75 (4-methylene-2-octyl-5-oxotetrahydrofuran-3-carboxylic acid). It is converted intracellularly by endogenous acyl-CoA synthetase to its CoA adduct, (±)-C75-CoA, a strong competitive inhibitor to CPT1 [16]. Its systemic administration in rats led to food intake decline, and body weight decrease, as the drug was shown to cross the BBB and get converted to (±)-C75-CoA in the ARC hypothalamic nucleus [17,19]. Makowski *et al* [8] performed the stereoselective synthesis of (+)-C75 [(2R,3S) isomer] and (-)-C75 [(2S,3R) isomer] to explain their differential pharmacological activities. (+)-C75 was found to be an anorectic by inhibiting CPT1 activity after conversion to (+)-C75-CoA. On the other hand, the effect of (-)-C75 in CPT1 activity is indirect, acting via FAS inhibition driving an increase in malonyl-CoA levels, which is the physiological inhibitor of CPT1. In addition, the effects of (-)-C75 without CoA adduct on food intake were negligible, but show antitumoral effects in several cell lines [8]. The presence of the CoA adduct in C75 is then crucial to exert inhibitory effect in CPT1, but it considerably reduces the uptake of the drug into the target cell. Therefore, strategies to C75 derivatives with intact CoA adduct into the target cells is needed. Since brain CPT1 is implicated in both cancer and obesity, the administration of (±)-C75-CoA and its enantio-separated CoA forms into specific brain cells presents a novel therapeutic strategy to treat both diseases.

The chemical structure of (±)-C75-CoA presents challenges to cellular entry. It is a small, polar, and charged metabolite, having low permeability across the cell membrane [20] and consequently needing a delivery system for intracellular transport. With its phosphate groups ionized at physiological pH, its anionic state, together with its long aliphatic side-chain enables CoA to interact with cation-conjugated polymers through a combination of electrostatic and hydrophobic interactions [21]. Therefore, forming a poly-ion complex (PIC) micelle with (±)-C75-CoA is a sound approach in designing a delivery system since it neutralizes the overall negative charge that would hinder its cellular entry. PIC micelles are well used various cargoes such as small, ionic molecules [22] and nucleic acids such as pDNA, mRNA, siRNA, and anti-sense oligonucleotides (ASOs) [23,24] with several relevant applications in GBM therapy [25] and neuron-targeted delivery [26].

The cationic polymer used is PEG-poly{N-[N'-(2-aminoethyl)-2-aminoethyl]aspartamide} (PEG-PAsp(DET)), which has a monoprotonated side chain at pH 7.4, at which point it only causes minimal membrane destabilization. At pH 5.5, the side chain becomes diprotonated, selectively destabilizing the endosomal membrane once inside the cell, enabling less toxic gene

transfer into cells [27,28]. This system has been used for mRNA transfection into neurons [29] as well as astrocytes and oligodendrocytes [30], making it an excellent candidate for (±)-C75-CoA delivery. We have successfully prepared a PIC micelle from PEG-PAsp(DET) that encapsulated (±)-C75-CoA and its enantio-separated forms. The micelles were tested on two brain-derived cell lines, U87MG human glioma cells and GT1-7 murine hypothalamic neurons, and we found that FAO and ATP synthesis were successfully inhibited in both. Using a model particle encapsulating a fluorescent CoA derivative, we were also able to demonstrate that the PIC micelle is efficiently taken up by both cell lines. This paper is the first report to describe the delivery of CoA-conjugated CPT1 inhibitors using PIC micelles to target CPT1 and modulate lipid metabolism in glioma cells and neurons.

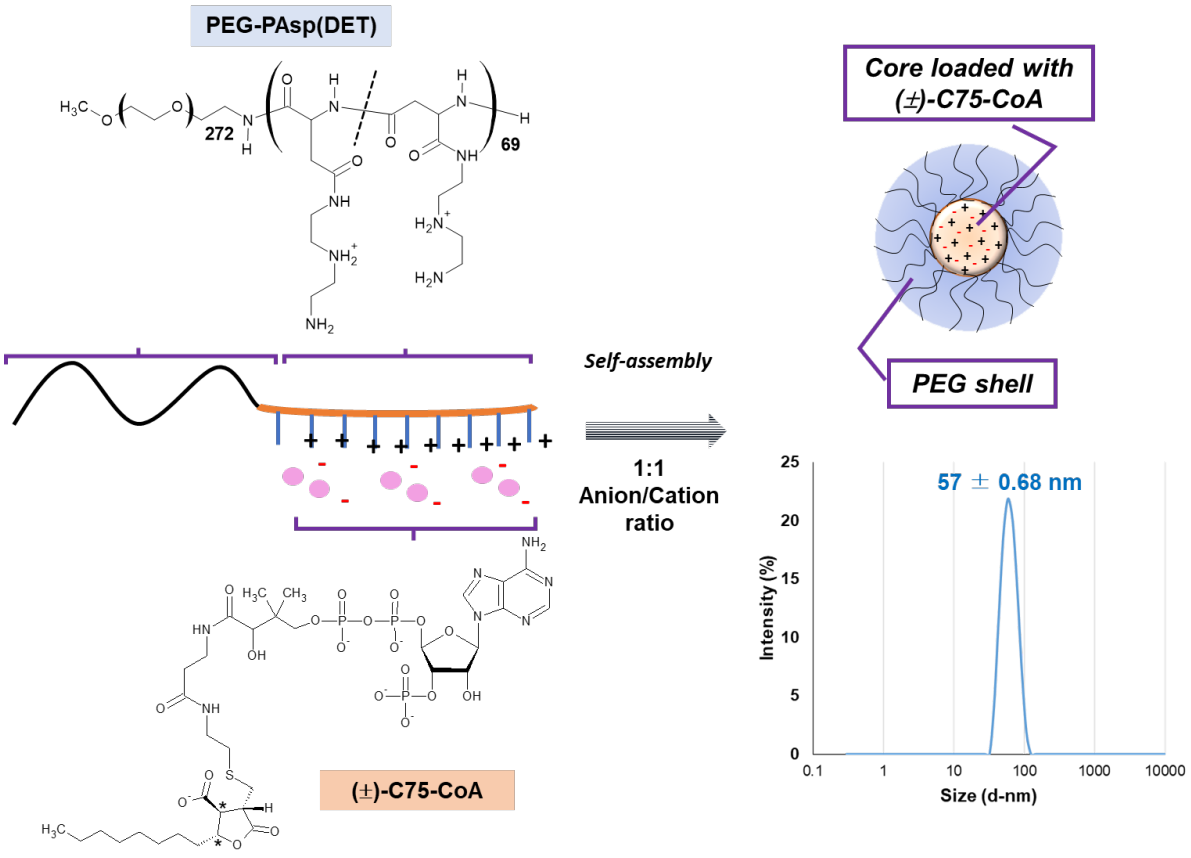

Scheme 1. Schematic of a poly-ion complex (PIC) micelle formation of (±)-C75-CoA with PEG-PAsp(DET), including its size distribution profile (hydrodynamic size vs intensity %).

2. RESULTS AND DISCUSSION

2.1 Preparation of C75-CoA micelles

The preparation of (±)-C75-CoA was carried out as previously described [17] (see detailed information in **ESI†**). On the other hand, enantioselective syntheses of (+)-C75 [(2R,3S) isomer] and (-)-C75 [(2S,3R) isomer] were performed by using enantiomeric chiral auxiliaries (**Figure S1, ESI†**). (±)-C75-CoA were formed by nucleophilic addition to the α,β-unsaturation of (±)-C75 by the ─SH group of CoA [8]. We confirmed the synthesis by comparing the ^{1}H NMR and HPLC profiles of the starting materials and product (**Figure S2, ESI†**). PEG-PAsp(DET) was prepared by anionic ring-opening polymerization of benzyl-L-aspartate *N*-carboxyanhydride (BLA-NCA) initiated from the terminal ─NH_2 group of PEG-NH_2 (MW 12,000) to form PEG-*b*-poly(β-benzyl-L-aspartate) (PEG-PBLA), and then subsequent aminolysis with diethylenetriamine (DET) (**Figure S3, ESI†**). The degrees of polymerization (DP) and substitution (DS) were measured from the ^{1}H NMR spectra. Using the proton peak intensity ratio of the PEG methylene protons (δ = 3.4-3.6 ppm) to the aromatic ring protons (δ = 7.1-7.5 ppm) in the polypeptide side chain of PBLA, DP was calculated to be 69. After aminolysis, the same PEG methylene protons were then compared with all the methylene protons in the DET side chains (δ = 2.7-3.6 ppm), and the DS was found to be 63.

We then mixed the aqueous solutions of (±)-C75-CoA and PEG-PAsp(DET) in a 1:1 anion/cation ratio in 10 mM phosphate buffer (PB) pH 7.4 to give 57-nm PIC micelles with a unimodal size profile and narrow polydispersity. The zeta potential (ZP) was also close to neutral, indicating appropriate balance of cationic and anionic components in the resulting micellar formulation (**Table 1, Scheme 1**). At pH 7.4, around 51% of the aminoethylene units in the PEG-PAsp(DET) side chain are protonated [27], this imparts a cationic charge to the block co-polymer for neutralizing the negative charge of the anionic cargo, forming PIC micelles. The PEG chain of the polymer (MW 12,000) was also crucial in imparting these measured physicochemical properties, decreasing aggregation tendency and maintaining a neutral surface charge.

(+)- and (-)-C75-CoA were synthesized from the same procedure as (±)-C75-CoA and their corresponding micelles were also successfully prepared, with near-similar physicochemical properties (**Table 1**). Additionally, micelles loaded with other CoA derivatives were prepared

in order to confirm the applicability of the delivery system to molecules with similar structures. First, we used commercially-available palmitoyl-CoA since its hydrophobic tail resembled that of (±)-C75 and their molecular weights were also numerically close. Indeed, micelle formation was observed based on DLS measurements. However, when we used CoA (767.5 g/mol) or malonyl-CoA (853.6 g/mol), micelle formation was not detected. The probable reasons are that their MWs were much smaller from (±)-C75-CoA and that they did not possess the characteristic hydrophobic moieties, despite having the phosphate groups necessary for PIC formation. This indicates that hydrophobicity was to some degree a part of the driving force for micelle formation. To determine the percentage of (±)-C75-CoA loaded inside the micelle, ultracentrifugation was used to remove the unencapsulated free drug. The ratio of the drug concentration in the upper fraction of the filter and the total drug added in the micelle preparation was calculated. From this, we ascertained that (±)-, (+)-, and (-)-C75-CoA micelles all have high drug encapsulation rates (above 80%). The ionic interaction between the drug and polymer was further confirmed by the statistically significant decrease in scattering light intensity and % encapsulation when (±)-C75-CoA micelle was mixed with concentrated salt solutions (0.5 and 1 M NaCl) (**Figure S4**, **ESI†**). This means that high NaCl concentrations disrupted the electrostatic interactions between the anionic groups of the cargo molecule and the cationic side chain of the polymer, leading to reduced micelle formation and increased free drug concentration outside the micelle.

Micelle	**MW (g/mol)**	**Size (d-nm)**	**Polydispersity**	**Zeta potential (mV)**	**Encapsulation (%)**
(±)-C75-CoA	1004	56.7 ± 0.68	0.06 ± 0.0037	-0.29 ± 1.98	84.2 ± 0.52
(+)-C75-CoA	1004	63.5 ± 1.45	0.05 ± 0.0082	-0.68 ± 2.25	82.2 ± 0.01
(-)-C75-CoA	1004	55.0 ± 0.38	0.02 ± 0.0232	0.17 ± 2.62	87.3 ± 0.03
Palmitoyl-CoA	1005.9	59.5 ± 0.69	0.02 ± 0.0017	2.37 ± 0.85	66. 8 ± 0.05
Fluorescein-CoA	1175.8	56.9 ± 0.16	0.04 ± 0.0070	0.38 ± 1.46	94.3 ± 0.18

Table 1. Physicochemical characteristics of (±)-C75-CoA, Palmitoyl-CoA and Fluorescein-CoA micelle. Experiments were performed in triplicate, with values expressed as mean ± SD.

Next, to evaluate its long-term stability in cold storage, the change in micelle characteristics was monitored every 7 days for a total of 28 days during storage at 4 °C (**Figure 2**). The purpose of this experiment was to ensure that micelles prepared in advance can still be used in biological assays after a few days of storage. One-way analysis of variance (ANOVA) revealed apparent linear relationships between each physicochemical parameter and incubation time. We observed micelle size to increase slightly with time ($R^2 = 0.9609$) (**Figure 2 a**). This increase in size was accompanied by a steady increase in scattering light intensity ($R^2 = 0.9984$) (**Figure 2 b**) as expected, indicating that no apparent decrease in particle concentration occurred. There was also no apparent change in PdI throughout the observation period (**Figure 2 c**). The size profile remained monodisperse, as the PdI remained well below 0.15, which was particularly narrow. ZP stayed close to neutral all throughout the observation period, despite a weak increase associated with time ($R^2 = 0.7432$) (**Figure 2 d**). However, there was no significant change between the initial and final values. Overall, despite the tendency to gradually change over time, it is reasonable to conclude that micelle integrity was maintained for 28 days in storage at 4 °C.

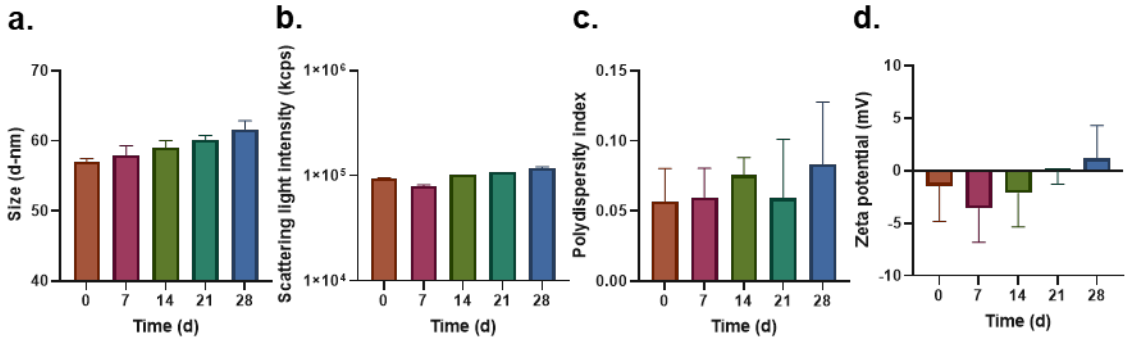

Figure 2. Long term stability studies of (±)-C75-CoA micelle, including measuring changes in physicochemical properties over 28 days in storage at 4 °C: size (a), scattering light intensity (b), polydispersity (c), and zeta potential (d). Experiments were performed in triplicate (values expressed in mean ± SD) and linear relationships were established using ANOVA.

2.2 Inhibition of fatty acid metabolism

2.2.1 ATP synthesis

Long-chain fatty acids (LCFAs) need to enter the mitochondria to undergo β-oxidation. They are first esterified into the LCFA-CoA form, which is shuttled into the mitochondria by CPT1

(**Figure 3 a**). Upon entry, the LCFA-CoA undergoes β-oxidation to form several acetyl-CoA molecules, which then enters the Krebs cycle. Acetyl-CoA is eventually degraded into CO_2, and in the process produces NADH, which enters the electron transport chain (ETC) to finally yield ATP [31,32]. By this pathway, FAO inhibition is known to impair ATP production. We examined whether C75-CoA will show this effect by measuring ATP concentration in cells after incubation with free and micellar C75-CoA (**Figure 3 b-c**) for 45 minutes. In general, the micelle effect is well-pronounced as the ATP concentrations from micelle-treated cells are significantly lower than those from free drug-treated groups. This suggests that the effective delivery of C75-CoA inside the cells led to a higher concentration of the compound reaching the mitochondria, further steering into a substantial inhibition of FAO by the nano-encapsulated drugs.

U87MG is the most widely used cell line for human glioma research [33]. It was also reported to express CPT1 [11], making it an appropriate model for our subsequent experiments. For U87MG, neither ETO nor the free drugs with CoA adduct, were able to effectively reduce ATP levels (**Figure 3 b**). Nevertheless, cells treated with (±)-, (-)- and (+)-C75-CoA micelles showed significant reduction in ATP levels compared to their corresponding non-encapsulated drugs. This ATP lowering effect is particularly appreciated with (-)-C75-CoA micelle, which was the most effective compared to all other groups. Although the lack of effect of ETO in ATP levels did not correlate with previous publications [34,35] , we observed a reduction in FAO assay with etomoxir in U87MG (**Figure 4 c**), confirming the inhibitory effect of this drug on mitochondrial metabolism, although the dosage-dependent off-target effects attributed to ETO could explain the result in ATP levels [36] .

GT1-7 is an immortalized murine hypothalamic neuronal cell line which is used in endocrinology and metabolism studies [37]. It was also reported to express CPT1 [38] and, since it is in our interest to measure CPT1 inhibition in the hypothalamus, this cell line is an appropriate *in vitro* model. ATP levels in GT1-7 were discernibly reduced in response to ETO and by the free (±)- and (-)-C75-CoA derivatives, but no changes were observed in the (+)-C75-CoA-treated group (**Figure 3 c**). Drug encapsulation led to a statistical enhancement in ATP reduction induced by both (+)- and (-)-C75-CoA forms. As shown in U87MG, (-)-C75-CoA micelle was still most effective in reducing ATP among all treatment groups including ETO.
A concurrent cell viability assay confirmed that the treatments in both U87MG and GT1-7 cells did not cause any apparent cell death, compared to the non-treated group (**Figure 3 d-e**). This

highlights one of the advantages of the delivery system that we used, since PEG-PAsp(DET) causes only minimal toxicity [27]. Although other cationic polymers like poly-(L-lysine) and poly(ethylenimine) (PEI) are well-used to deliver anionic molecules, their toxicity upon micellar disassembly limits their biological applications [39]. Overall, our results verify that for both cell types, the micelles were more successful in reducing ATP synthesis as compared to the free drug without causing excessive cell death.

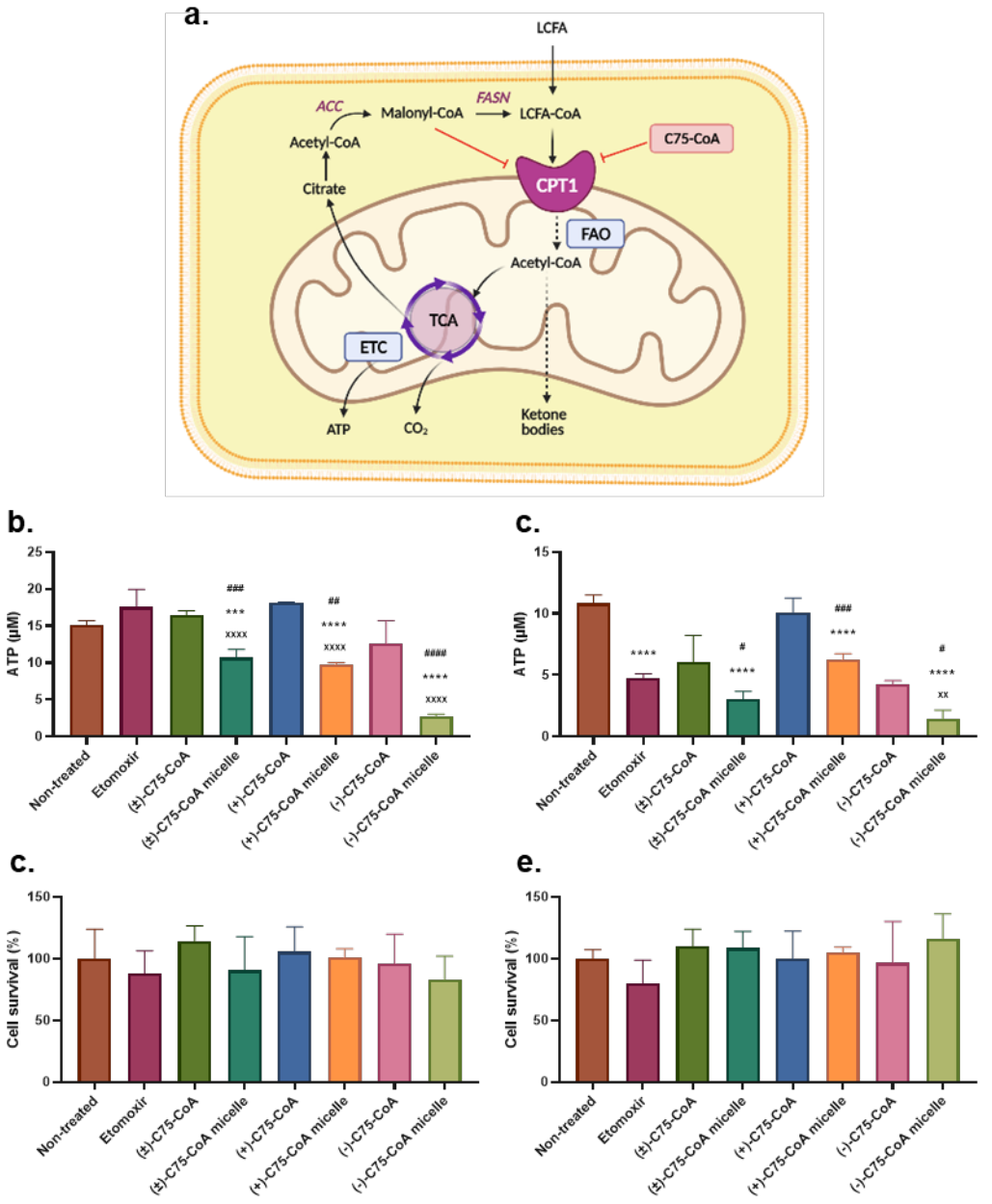

Figure 3. Illustration of ATP generation from LCFA metabolism (a). Levels of ATP produced by U87MG (b) and GT1-7 (c) after treatment with FAO inhibitors. Simultaneous Calcein AM cell viability assay for U87MG (d) and GT1-7 (e) using the same conditions and treatments as ATP assay. Experiments were performed in quadruplicates (values expressed in mean ± SD) and comparison of means among treatment groups were done using ANOVA (with Tukey's test as post-hoc analysis; ***P<0.001, ****P<0.0001 versus

non-treated cells; ^{xx}P<0.01, ^{xxxx}P<0.0001 versus etomoxir; $^{\#}$P<0.05, $^{\#\#}$P<0.01, $^{\#\#\#}$P<0.001, $^{\#\#\#\#}$P<0.0001 versus the corresponding free form of C75-CoA.).

2.2.2 FAO assay

Palmitate oxidation in both U87MG and GT1-7 cells was evaluated in terms of: oxidation to CO_2 (**Figure 4 a & d**), conversion to acid-soluble products (ASPs) such as ketone bodies (**Figure 4 b & e**) and total FAO rate calculated as the sum of ASP plus CO_2 oxidation (**Figure 4 c & f**). The final fate of palmitate oxidation in both cell types was significantly different. In particular, most of palmitate oxidation levels measured in U87MG cells come from ASPs (ranging 7.5 nmol/mg prot/h), with minimal contribution of oxidation to CO_2 (ranging 0.1 nmol/mg prot/h), whereas GT1-7 cell lines showed more equitable contribution of palmitate oxidation to ASPs and CO_2 total FAO. The differences in palmitate oxidation fate between glioblastoma or neuronal cell lines agree with previous publications indicating the different metabolic profile of both cell types [34,40–42] .

In U87MG cells, ETO effectively reduced FAO to CO_2 and ASP (**Figure 4 a-c**), since ASP oxidation was the main pathway contributing to total reduction of FAO. In contrast, the free forms of C75-CoA were unable to modify these oxidation parameters compared to non-treated cells. Nano-encapsulation of the three forms of C75-CoA, led to a substantial attenuation of total FA oxidation (**Figure 4 c**), reaching similar levels to ETO-treated cells, and these changes were due to palmitate oxidation to ASP (**Figure 4 b**), probably reducing the generation of TCA intermediary metabolites and ketone bodies crucial for glioblastoma cells proliferation [34,40] . Similar levels of FAO attenuation were reached in (±)-, (+)- and (-)-C75-CoA micelles-treated U87MG cells (**Figure 4 c**).

In GT1-7, ETO was also able to reduce FAO oxidation, whereas palmitate oxidation remained unchanged after treatment with the non-encapsulated C75-CoA forms in line to previous results (**Figure 4 d-f**). Nano-encapsulation of the C75-CoA derivatives induced a significant attenuation in total FAO, being the contribution of both palmitate fates, to CO_2 and ASP, similar to total oxidation of FA (**Figure 4 d-f**). Cells treated with (±)-C75-CoA micelle showed the highest reduction in FAO compared to non-treated conditions, reaching similar levels to those induced by etomoxir (**Figure 4 c**).

Altogether, our results indicate that nano-encapsulation of C75-CoA derivatives implies a substantial improvement in FAO inhibition by these drugs in both U87MG and GT1-7 cell lines. We have also evidenced the differential contribution of either CO_2 or ASPs to FA oxidation in both cell lines, in agreement with the literature. Considering the recently identified role of FAO as a metabolic node in the aggressive phenotype of glioma cell lines [34,35], and the significant role of FA oxidation and CPT1 in neuronal metabolism and survival [38,42], the improved FAO inhibition showed by these micelles indicate the potential of these nanoparticles to modify brain metabolism in associated diseases such as cancer.

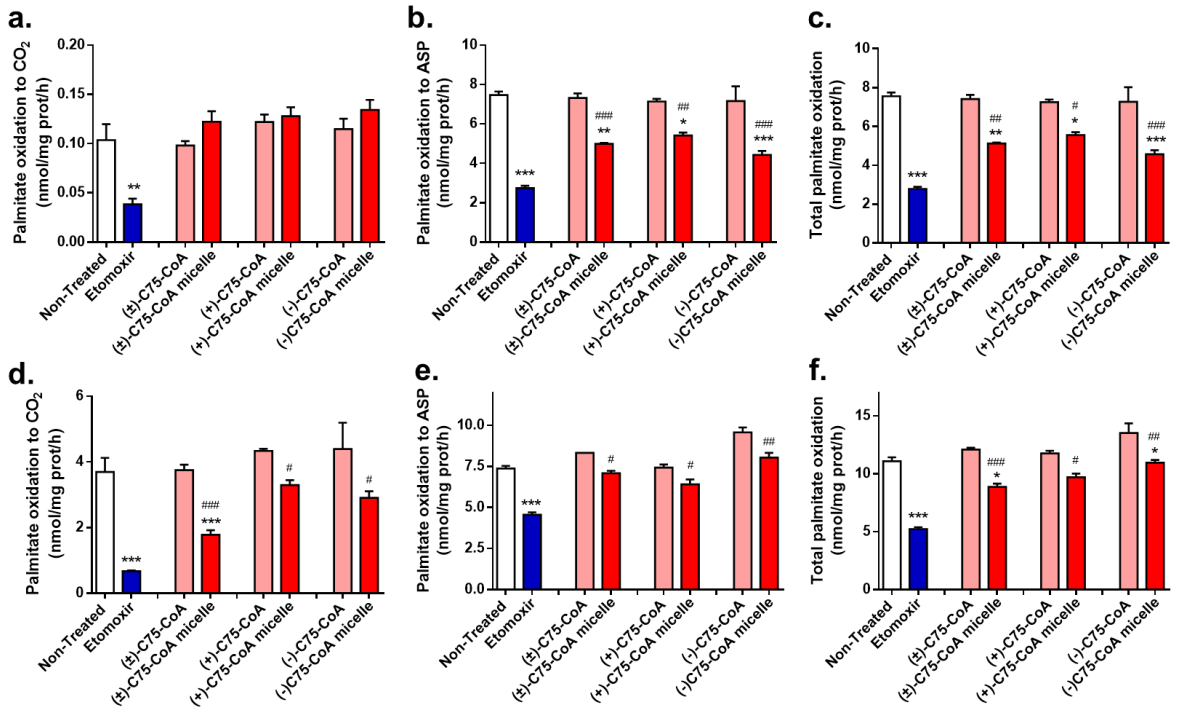

Figure 4. FAO oxidation in U87MG (a-c) and GT1-7 (d-f) cells after treatment with C75-CoA derivatives in free form or nano-encapsulated in micelles. ETO was used as positive control of FAO inhibition. FAO is represented as palmitate oxidation to CO_2 (a, d), ASP (b, e), and total palmitate oxidation (CO_2 + ASP; c, f). Results are the mean ± SD of two independent experiments performed by biological triplicates (n=5-6 samples per condition). Comparison of means were done using ANOVA followed by Tukey's comparison test; *P<0.05, **P<0.01, ***P<0.001 versus non-treated cells; #P<0.05, ##P<0.01, ###P<0.001 versus the corresponding form of C75-CoA.

2.3 Cytotoxicity of C75-CoA micelles

Since GB cells overexpress CPT1 [11,13] to increase their chances of survival, inhibiting this enzyme would negatively affect their proliferation. We incubated free and micellar C75-CoA with U87MG for 72 h, with ETO as a comparison drug. The drug and micelle-produced responses generally followed a sigmoidal shape (**Figure 5 a-d**). C75-CoA (racemic and

enantio-separated forms) is overall significantly more cytotoxic to the respective free drug (**Figure 5 e**). Notably, the mean IC_{50} of free (±)-C75-CoA was decreased 4-fold when delivered in micelle form. After 72 h, the difference between the mean IC_{50} of (±)- and (-)-C75-CoA micelles are not statistically significant, however, (+)-C75-CoA micelle is discernibly less cytotoxic than (±)-C75-CoA micelle. Free (+)-C75-CoA is less cytotoxic than ETO. On the other hand, ETO shows comparable toxicity to (±)- and (-)-C75-CoA micelles despite being a free drug, owing to other mechanisms outside of CPT1 inhibition such as production of reactive oxygen species [32,43].

Two-way ANOVA revealed that the mean IC_{50} values of all FAO inhibitors were all found to decrease with time in a linear fashion ($R^2 > 0.9$). The cytotoxicity of (±)-C75-CoA micelle was demonstrated to be more pronounced at longer incubation periods, approaching comparable values as ETO after 72 h (**Figure 5 f**). Note that decrease in cell viability is achieved only upon lengthier exposure, since the 45-min incubation in the ATP assay (**Figure 3 c**) was not enough to kill the cells. Cellular morphologies were also retained after short-term incubation with both free and micellar (±)-C75-CoA in the FAO assay (**Figure S5, ESI†**). These results provide the initial evidence to support the further development of these PIC micelles as a therapeutic platform against GBM. It also shows that the delivery of (±)-C75-CoA inside the cell is important in amplifying its growth inhibitory properties. Given its anionic state, it is assumed to have limited permeability across the cell membrane [20], with the micelle state neutralizing this negative charge and promoting its transport into the cell through endocytosis.

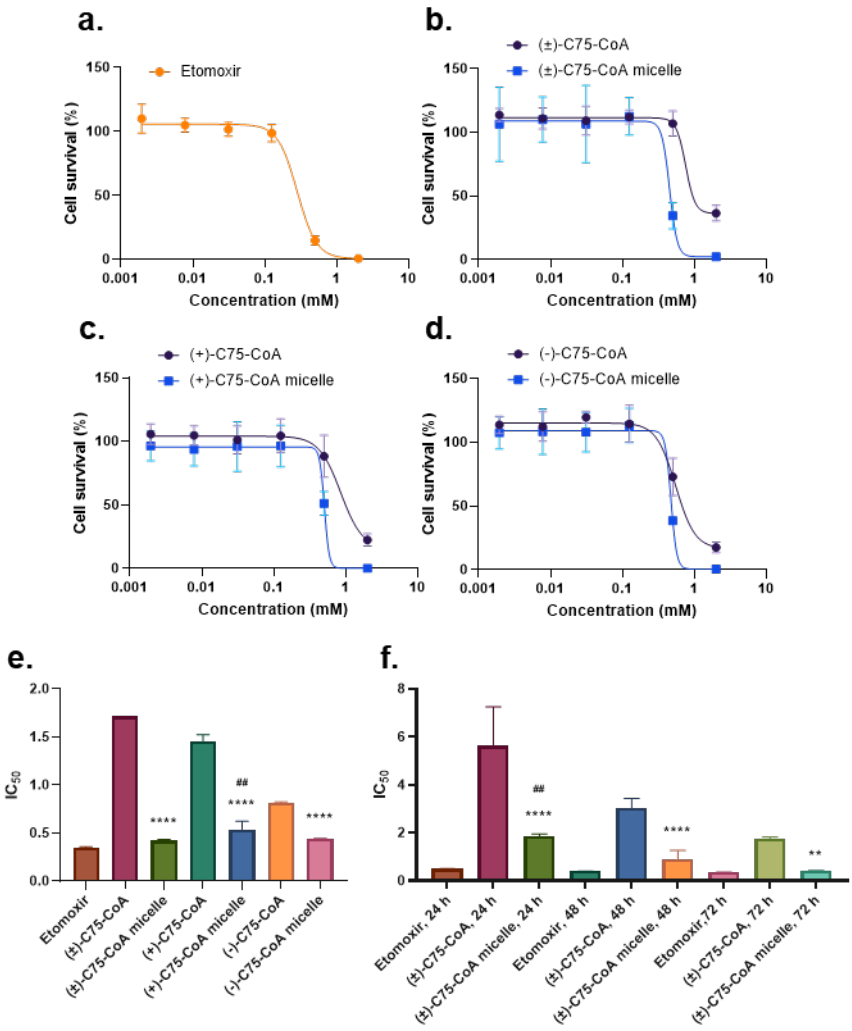

Figure 5. Cytotoxicity of FAO inhibitors on U87MG at 72 h incubation, including the dose-response curves of ETO (a) and the free vs micelle forms of (±)-C75-CoA (b), (+)-C75-CoA (c), and (-)-C75-CoA (d). IC_{50} of ETO, free. and micelle forms of (±)-, (+)-, and (-)-C75-CoA at 72 h incubation (e) and only for (±)-C75-CoA at 24-, 48-, and 72-h incubation periods (f). Experiments were performed in triplicates (n=4 samples per condition; values expressed in mean ± SD) and comparison of means among treatment groups were done using one-way ANOVA (with Tukey's test as post-hoc analysis; **P<0.01, ****P<0.001 versus the corresponding form of C75-CoA; $^{\#\#}$P<0.01 versus etomoxir).

2.4 Quantification of cellular uptake using Fluorescein-CoA encapsulated PIC micelle

To confirm that PIC micelle type system facilitated cellular uptake of CoA-conjugated (±)-C75 by neutralizing the negative charges, we synthesized a fluorescein analogue of CoA (Fluorescein-CoA; herein Fluor-CoA) and encapsulated it inside the PIC micelle. Fluor-CoA was prepared by simple maleimide chemistry starting from fluorescein-5-maleimide. The resulting compound had a MW (1175.8 g/mol) close to (±)-C75-CoA (1004 g/mol), including the same number of carboxylate and phosphate groups, which therefore imparted analogous physicochemical properties. The addition of fluorescence emission ($\lambda_{excitation}$ = 475-490 nm,

$\lambda_{emission}$ = 510-520 nm) made cellular uptake studies using confocal microscopy or flow cytometry possible. The ─SH group of CoA added to the maleimide ring of fluorescein-5-maleimide to give the desired product (**Figure S6 a, ESI†**), which we confirmed by comparing the ^{1}H NMR and HPLC profiles of the starting materials and product (**Figure S6 b-c, ESI†**). In the chromatogram, the Fluor-CoA peak is revealed by both the fluorescence and UV absorbance (λ_{max} of CoA) detectors. In a similar fashion to (±)-C75-CoA, the aqueous solution of Fluor-CoA was combined with PEG-PAsp(DET) in a 1:1 anion/cation ratio in 10 mM phosphate buffer (PB) pH 7.4 to give 50-nm micelles with a narrow polydispersity (**Table 1**).

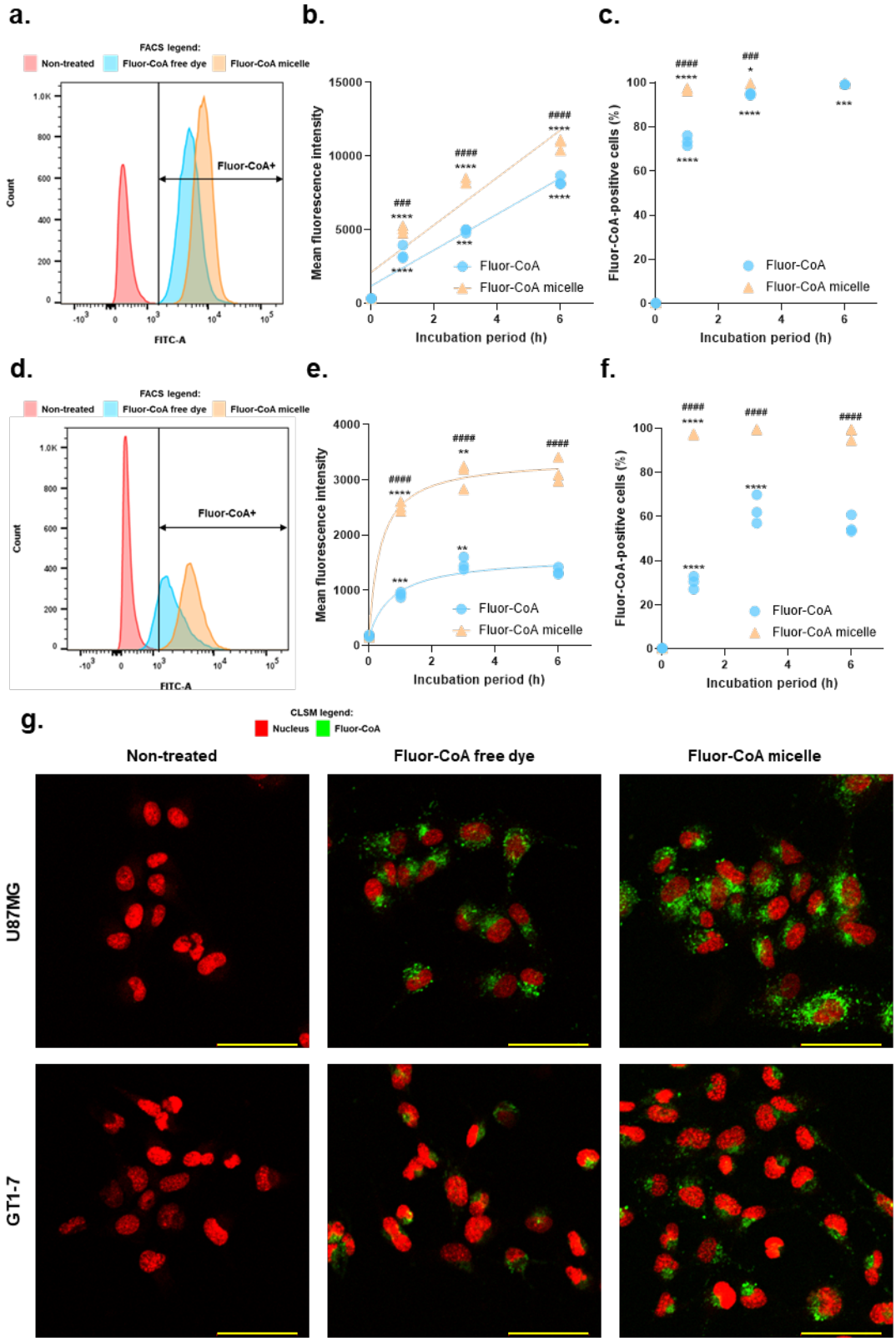

Figure 6. Analysis of cellular uptake of Fluor-CoA micelles vs free dye using CLSM and flow cytometry. U87MG data (a-c) are presented as sample histogram (a), mean fluorescence intensity (b), and percentage of Fluor-CoA-positive cells (c). GT1-7 data (d-f) are presented as sample histogram (d), mean fluorescence intensity (e), and percentage of Fluor-CoA-positive cells (f). Experiments were performed in triplicate (values expressed in mean ± SD) and comparison of means among treatment groups were done using ANOVA (with Tukey's test as post-hoc analysis; *P<0.05, **P<0.01, ***P<0.001, ****P<0.0001 vs measurement at preceding time point; $^{###}$P<0.001, $^{####}$P<0.0001 vs corresponding free Fluor-CoA).

Representative confocal microscopy images (g) of U87MG and GT1-7 after 1 h incubation with Fluor-CoA free dye and micelle. Scale bar = 50 µm, magnification 5×.

Cellular uptake in both U87MG and GT1-7 was visualized using confocal laser scanning microscopy (CLSM) and quantified using flow cytometry (**Figure 6**). We incubated the micelles with the cells at different time points (1, 3, or 6 h) and at a fixed concentration of Fluor-CoA micelle (0.25 mg/mL), which contained 0.1 mg/mL free dye. The equivalent Fluor-CoA concentration was therefore used in the free dye-treated groups. In flow cytometry, only DAPI-stained cells were counted in order to exclude interference from dead cells. The data we obtained included mean fluorescence intensity (MFI), to indicate extent of micelle internalization, and percentage of Fluor-CoA+ cells after gating, to quantify the % of cell population in which the free or micellar Fluor-CoA have entered.

Internalization of both free dye and micelle increased with time in both cell types (**Figure 6**). Mutually, micellar uptake in terms of MFI was statistically higher than free dye uptake, at all measured time points (**Figure 6 b & e**). In addition, the values for %Fluor-CoA+ cells were discernibly greater for the micelle compared to the free dye, for both cell lines (**Figure 6 c & f**). Even after 1 h of incubation, the micelles have entered more than 95% of the cells. Specifically, for U87MG, MFI corresponding to micelle uptake was 1.5-fold elevated, on average, compared to that of the free dye (**Figure 6 b**). We found that cellular uptake displayed a strong linear increased over time for both micelle ($R^2 = 0.8708$) and free dye ($R^2 = 0.9394$). This meant that the cells were expected to continue internalization beyond the 6-h observation period. In terms of %Fluor-CoA+ cells, free dye uptake started at only 70% (1 h) but gradually increased and eventually matched the corresponding value for the micelle at 6 h (**Figure 6 c**). However, the micelle-treated cells still produced a higher fluorescence signal, signifying that the overall amount of Fluor-CoA delivered to the cells was higher. Mo *et al* [44] has previously described the tendency of U87MG to internalize polymeric NPs at a steady linear rate up to 6 h, which supports our findings.

The difference between micellar and free Fluor-CoA uptake was more amplified in GT1-7. MFI of micelle uptake was around 2 to 3 times higher than free dye uptake through all the time points that we measured, which clearly indicated the penetration-enhancing effects of the micelle (**Figure 6 e**). In terms of %Fluor-CoA+ cells, the uptake started from 30% at 1 h, doubled at 3 h, and then plateaued (**Figure 6 f**). Unlike in U87MG, the rates of internalization did not increase in a linear fashion but fit a non-linear model called the Padé (1,1) approximant

(Fluor-CoA R^2 = 0.9493; Fluor-CoA micelle R^2 = 0.9870). In addition, the free drug entered only around 60% of the cell population even at a 6-h incubation period, never quite reaching the 98% uptake that the micelle has attained after only 1 h of incubation. The saturable uptake of PEGylated polymeric micelles has previously been previously demonstrated for neurons by Rabanel *et al* [45] who attributed it to their limited capacity to accommodate NPs.

Multi-cellular spheroids were generated by seeding cells in low-adhesion plates and allowing them to form clusters by secreting their own extra-cellular matrix (ECM) [46], which provides additional penetration barriers for the NPs [47], therefore more accurately modeling the *in vivo* environment as compared to the monolayer culture. We found that micellar internalization was also higher compared to the free dye in U87MG and GT1-7 spheroids (**Figure S7, ESI†**), suggesting that even in a 3D model with additional barriers, our above findings in the monolayer hold true.

3. CONCLUSION

We have successfully prepared PIC micelles loaded with the CPT1 inhibitors (±)-, (+)-, and (-)-C75-CoA. The cationic block-copolymer PEG-PAsp(DET) provided a platform by neutralizing the negative charge of the cargo molecules, generating micelles with physicochemical properties (50-60 nm size range and neutral surface charge) that are stable in long term storage. Through targeting CPT1, FAO was effectively impeded, which led to overall decreased metabolism of ^{14}C-palmitate into CO_2 and acid-soluble products. We found that these results were consistent with the ATP inhibition experiments, where ATP production in both U87MG and GT1-7 was diminished up to 5-folds by the micelles, in comparison with the free drug counterparts. During these short-term incubation experiments, no apparent decrease in viability was induced by the micelles. When we assayed the cytotoxicity in glioma cells after longer incubation periods, C75-CoA micelles inhibited cell growth more discernibly compared to the free drug forms, where IC_{50} was reduced 2 to 4-folds. (±)- and (-)-C75-CoA micelles even showed comparable efficacy to the known FAO inhibitor etomoxir. The fluorescent dye model particle, Fluor-CoA micelle, showed a statistically increased internalization in both cell lines as well, in comparison with the free dye, reaching a 2 to 3-fold increase especially in GT1-7 neurons. This corroborated the cytotoxicity and FAO inhibition results – delivery through PIC micelle resulted in increased cellular concentration of the cargo, which led to increased biological activity. Although internalization was generally time-dependent, we

showed that the micellar uptake kinetics differed between the cell lines. This PIC micelle has previously been reported to be effective in gene delivery to brain cells including glial cells like astrocytes and oligodendrocytes [30] as well as neurons [29]. From our data, we can compellingly conclude that uptake in neuronal and glioma cells of small anionic cargoes like Fluor-CoA and by extension, C75-CoA, is thoroughly improved by using a PIC micelle. Additionally, the advantage of using a micelle-type delivery system was more pronounced for the neurons as compared to the glioma cells. Drug delivery into neurons are generally more challenging compared to other cells and this is reflected in the fact that there is a lack of neuron-targeted delivery systems present in the clinic [26]. Our results contribute to the growing pool of knowledge on glioma- and neuron-targeted delivery, therefore warranting further development into effective brain therapeutics which especially involve the delivery of CPT1 inhibitors and other negatively-charged molecules for management of diseases where modulating lipid metabolism is a key emerging strategy.

4. MATERIALS AND METHODS

4.1 Synthesis of (±)-C75-CoA, (+)-C75-CoA and (–)-C75-CoA

The preparation of (±)-C75-CoA was carried out as previously described [17] (see detailed information in ESI†). Enantioselective synthesis of (+)-C75 and (–)-C75 was performed by using enantiomeric chiral auxiliaries (**Figure S1, ESI†**).

4.2 Synthesis of PEG-PAsp(DET)

The preparation of PEG-PBLA through NCA ring-opening polymerization was carried out as previously reported [48]. Subsequent aminolysis of the polymer with DET was carried out also as described earlier [27,28]. See detailed information in ESI†.

4.3 Preparation and characterization of PIC micelles

PEG-PAsp(DET) was dissolved in 10 mM phosphate buffer pH 7.4 at 10 mg/mL concentration by overnight stirring at 4 °C. After which, the solution was passed through using 0.22-μM filter. The polymer and (±)-C75-CoA solutions were mixed in a 1:1 anion-to-cation ratio, vortexed, and then again filtered (0.22-μM) under sterile conditions prior to succeeding experiments. For

DLS measurements (Zetasizer Ultra, Malvern Panalytical, Spectris plc, UK), micelle suspensions were diluted to 1 mg/mL and placed inside a ZEN2112 quartz cuvette. Light scattering data was measured using a 50-mW 532 nm DPSS laser incident beam at a detection angle of 173° with a He-Ne laser 633 nm at 25 °C. The autocorrelation function produced was analyzed through the cumulant approach. Size is expressed as the hydrodynamic diameter, which was calculated with the Stokes−Einstein equation. Attenuator selection was automated. For zeta potential measurements, micelle suspensions were introduced in a ZEN1010 HC cell, using the Smoluchowski approach. During stability studies, micelles were kept at 4 °C and measurements were repeated every 7 d for 28 d in total.

4.4 Quantification of drug inside PIC micelles

Micelle solutions were pipetted into Amicon Ultra-0.5 mL centrifugal filters (MWCO 10,000, Merck Millipore, cat. # UFC501096) and spun (14,000 g, 15 min, 4 °C). The filtrate was then collected, weighed, and then transferred into UV-transparent 96-well plates. Its absorption at λ_{max} CoA = 259 nm was measured using a microplate reader (Infinite® M1000 Pro, Tecan Trading AG, Switzerland). Drug encapsulation was calculated by getting the ratio of the filtrate absorbance to that of the original (±)-C75-CoA solution added to form the micelle.

4.5 Cell cultures and treatments

Glioblastoma U87MG cell line (Merk Millipore, Sigma, Madrid, Spain) was cultured in DMEM (4.5 g/L glucose) supplemented with 10% FBS and murine hypothalamic neuronal cells GT1-7 (Merk Millipore, Sigma, Madrid, Spain) were cultured in DMEM (4.5 g/L glucose) supplemented with 10% FBS, 4 mM L-glutamine, 1% penicillin-streptomycin, and 1 mM sodium pyruvate at 37 °C in a humidified atmosphere of 95% air and 5% CO_2.

4.6 Cytotoxicity assays

In vitro cytotoxicity of etomoxir (ETO, Cayman, cat. # 11969) and free and micellar C75-CoA derivatives (racemic and enantiopures with CoA adduct) were evaluated against human GB cell lines and U87MG. The cells (3×10^4 cells / well) were seeded in a 96-well plate using DMEM (Sigma-Aldrich, cat. # D6429) containing 10% FBS in 96-well-plates 24 h prior to the assay. The cells were then incubated with the test solutions. Cell viability was measured after

24, 48, and 72 h of exposure, by using cell-counting kit-8 (CCK8) (Dojindo, cat. # CK04) by measuring the product absorbance at λ_{max} = 450 nm using a microplate reader (Infinite® M1000 Pro, Tecan Trading AG, Switzerland).

4.7 Synthesis of Fluor-CoA and preparation of Fluor-CoA micelles

Synthesis of Fluor-CoA has been adopted from a previous protocol [49]. Briefly, 11.1 mg CoA sodium salt hydrate was dissolved in 100 µL 10 mM phosphate buffer pH 7.4. To this, 4.8 mg fluorescein-5-maleimide (TCI, cat. # F0810) in 900 µL DMF was added. The reaction mixture was stirred overnight at 30 °C. After which, benzene was added the resulting mixture, flash-frozen using liquid N_2 and then dried *in vacuo*. To confirm product formation, the same HPLC procedure was performed as in (±)-C75-CoA, but in addition to UV absorption at λ_{max} CoA = 259 nm and λ_{max} fluorescein = 460 nm, fluorescence detection ($\lambda_{excitation}$ = 494 nm, $\lambda_{emission}$ = 521 nm) was added. The HPLC peak passing all the detection criteria corresponds to the compound with both CoA and fluorescein moieties. PEG-PAsp(DET) and Fluor-CoA solutions were mixed in a 1:1 anion-to-cation ratio, vortexed, and then again filtered (0.22-µM) under sterile conditions.

4.8 Measurement of ATP levels

Measurement of ATP levels in parallel to cell viability assays were performed according to a previously reported procedure [32]. Produced ATP was quantified using a luminescence assay. Cells (2×10^5 cells/well) were seeded in a white, flat-bottom 96-well tissue culture plate 24 h prior to the assay. The cells were then incubated with ETO, C75-CoA, and C75-CoA micelle (0.5 mM) in bicarbonate-free DMEM (Sigma-Aldrich, cat. # D5030) supplemented with 2.5 mM glucose (Gibco, cat. # A2494001) and 275 nM oleate-BSA (Sigma-Aldrich, cat. # O3008) for 45 minutes in a separate incubator with 0% CO_2. The assay was then performed according to manufacturer protocol (CellTiter-Glo® Luminescent Cell Viability Assay, Promega, cat. # G9241). A calibration curve for ATP (TCI, cat. # A0157) was prepared. Luminescence signal for 10s were measured in each well using GloMax® Multi Detection System (Promega Corp, Madison, Wisconsin).

For the relative cell viability Calcein AM cell staining was performed. The relative viability was determined using the Calcein AM assay. In parallel to the ATP assay, cells (2×10^4

cells/well) were seeded in a white 96-well tissue culture plate 24 h prior to the assay. The cells were then incubated with ETO, C75-CoA, and C75-CoA micelle (1 mM) in bicarbonate-free DMEM (with 25 mM glucose and 6 mM glutamine) for 45 minutes in a separate incubator with 0% CO_2. The assay was then performed according to manufacturer protocol (Calcein AM; Invitrogen). Calcein AM was added to each well 30 min before measuring fluorescence intensity ($\lambda_{excitation}$ = 495 nm, $\lambda_{emission}$ = 515 nm) using a microplate reader (Infinite® M1000 Pro, Tecan Trading AG, Switzerland). Viability was normalized against non-treated cells.

4.9 Measurement of FAO inhibition

Palmitate oxidation to CO_2 and acid-soluble products (ASPs), essentially acyl-carnitine, Krebs cycle intermediates, and acetyl-CoA, were measured in U87 and GT1-7 cell lines grown in 12-well plates. Cells were treated with ETO, C75, C75-CoA (racemic and enantiomers), and C75-CoA micelle (racemic and enantiomers) (1 mM) in DMEM (4.5 g/L glucose) for 45 minutes. The day of the assay, cells were washed in KRBH-0.1% BSA, preincubated for 30 min at 37°C in KRBH-1% BSA. Cells were then incubated for 3 h at 37°C with fresh KRBH containing 2.5 mM glucose and 80 nM of labeled palmitate per well. Oxidation was measured as described [50] . The scintillation values were normalized to the protein content of each well and the result for CO_2 and ASPs are expressed as previously described [50] .

4.10 Confocal laser scanning microscopy (CLSM)

Confocal images were taken using an LSM880 confocal microscope (Carl Zeiss, Oberkochen, Germany) at a magnification of 5× using white light, 488- and 633-nm lasers for $\lambda_{excitation}$ of Fluor-CoA and NucSpot® 650, respectively. U87MG and GT1-7 cells (6×10^4 cells / well) were seeded in µ-slide 8-well chambered coverslip (ibidi, cat. # 80826) 24 h prior to observation. Cells were then incubated with 100.0 µL nanoparticle suspension in medium (0.25 mg Fluor-CoA micelle/mL containing 0.1 mg Fluor-CoA/mL) as well as NucSpot® 650 (Biotium, cat. # 40082) as nuclear stain (1 µL/mL suspension) and Verapamil HCl as efflux pump inhibitor (1 µL/mL suspension) for 1 h. Cells were then washed 2 × with PBS (-) before replacing medium with DMEM containing Trypan Blue (0.5 µL/mL) to quench fluorescent dyes attached on the cell surface.

4.11 Quantification of cellular uptake using FACS

U87MG and GT1-7 cells (3×10^5 cells / well) were seeded in 6-well plates 24 h prior to the assay. Cells were then incubated with nanoparticle suspension in medium (0.25 mg Fluor-CoA micelle/mL containing 0.1 mg Fluor-CoA/mL) with varying incubation times (1, 3, and 6 h). Nanoparticle suspension was washed twice with 1 mL PBS (-) and then incubated with 300 µL Accutase® Cell Detachment Solution (Innovative Cell Technologies, San Diego, California) for 3 minutes at 37 °C. The cells were then collected by adding 1 mL PBS (-) and transferring to a 25-mL plastic tube (I use 25 mL-tube). The cell suspension was then centrifuged at 300 g for 5 mins at 4 °C. The cells were further washed twice with PBS (-) and twice with 2% FBS in PBS (-). After final washing, the cells were resuspended in 500 µL of 1 µg/mL DAPI in 2% FBS in PBS (-) to stain live cells, then passed through a cell strainer and kept on ice. Mean fluorescence intensity and percentage of Fluor-CoA+ cells in FITC channel were measured by flow cytometry (BD LSRFortessa™ Flow Cytometer, BD Biosciences, San Jose, California) using FSC and SSC detection to gate out debris, and the UV (355 nm) and blue lasers (488 nm) for the detection of DAPI and Fluor-CoA, respectively. Data analysis was performed using FlowJo software (BD Biosciences, San Jose, California).

For spheroid culture, cell suspensions (50 µL) were seeded into each well (1000 cells/well) of a low-adhesion Prime Surface™ 96-well U-bottom plate (Sumitomo Bakelite Co., Japan) and incubated for 3 d. Images were taken using Keyence All-In-One Fluorescence Microscope BZ-X710 (Keyence Corp, IL). Cells were then incubated with nanoparticle suspension (50 µL) in medium (final concentration: 0.25 mg Fluor-CoA micelle/mL containing 0.1 mg Fluor-CoA/mL) for 3 h. Cells were then harvested using a pipette and collected into a 25-mL plastic tube. Washing and analysis were performed as above.

4.12 Statistical analysis

Data are expressed as means ± SD of assays performed at least triplicates. Several statistical analyses were performed using GraphPad v8: (1) statistical significances were determined Student's t-test (column analysis), one-way ANOVA with Tukey's post-hoc (grouped analysis), or two-way ANOVA and (2) relationships between variables were analyzed using linear and non-linear regression using the same software.

ACKNOWLEDGEMENTS

This project was financially supported by the Joint Bilateral Project Japan-Spain (PCI2018-092997/Agencia Estatal de Investigación (AEI) and 20jm0210059h0003/ Agency for Medical Research and Development (AMED), the Japan Society for Promotion of Science (JSPS) Bilateral Joint Research Projects (JPJSBP120209938), the Center of Innovation (COI) Program (JPMJCE1305) from Japan Science and Technology Agency (JST). The authors have no other relevant affiliations or financial involvement with any organization or entity with a financial interest in or financial conflict with the subject matter or materials discussed in the manuscript apart from those disclosed. No writing assistance was utilized in the production of this manuscript.

REFERENCES

1 K. D. Bruce, A. Zsombok and R. H. Eckel, *Front. Endocrinol. (Lausanne).*, 2017, **8**, 1–11.
2 J. A. Hamilton, C. J. Hillard, A. A. Spector and P. A. Watkins, in *Journal of Molecular Neuroscience*, Springer, 2007, vol. 33, pp. 2–11.
3 E. Currie, A. Schulze, R. Zechner, T. C. Walther and R. V. Farese, *Cell Metab.*, 2013, **18**, 153–161.
4 H. Rupp and A. Zarain-Herzberg, *Expert Opin. Investig. Drugs*, 2002, **11**, 345–356.
5 N. Casals, V. Zammit, L. Herrero, R. Fadó, R. Rodríguez-Rodríguez and D. Serra, *Prog. Lipid Res.*, 2016, **61**, 134–148.
6 M. J. Wolfgang, T. Kurama, Y. Dai, A. Suwa, M. Asaumi, S.-I. Matsumoto, S. H. Cha, T. Shimokawa and M. Daniel Lane, *Proc. Natl. Acad. Sci.*, 2006, **103**, 7282–7287.
7 A. Pocai, T. K. T. Lam, S. Obici, R. Gutierrez-Juarez, E. D. Muse, A. Arduini and L. Rossetti, *J. Clin. Invest.*, 2006, **116**, 1081–1091.
8 K. Makowski, P. Mera, D. Paredes, L. Herrero, X. Ariza, G. Asins, F. G. Hegardt, J. García and D. Serra, *Chirality*, 2013, **25**, 281–287.
9 M. López, C. J. Lelliott and A. Vidal-Puig, *BioEssays*, 2007, **29**, 248–261.
10 S. Obici, Z. Feng, A. Arduini, R. Conti and L. Rossetti, *Nat. Med.*, 2003, **9**, 756–761.
11 T. Wakamiya, S. O. Suzuki, H. Hamasaki, H. Honda, M. Mizoguchi, K. Yoshimoto and T. Iwaki, *Neuropathology*, 2014, **34**, 465–474.
12 P. T. Reilly and T. W. Mak, *Clin. Cancer Res.*, 2012, **18**, 5850–5855.
13 A. Cirillo, A. Di Salle, O. Petillo, M. A. B. Melone, G. Grimaldi, A. Bellotti, G. Torelli, M. S. De' Santi, G. Cantatore, A. Marinelli, U. Galderisi and G. Peluso, *Cancer Biol. Ther.*, 2014, **15**, 735–41.
14 K. Zaugg, Y. Yao, P. T. Reilly, K. Kannan, R. Kiarash, J. Mason, P. Huang, S. K. Sawyer, B. Fuerth, B. Faubert, T. Kalliomäki, A. Elia, X. Luo, V. Nadeem, D. Bungard, S. Yalavarthi, J. D. Growney, A. Wakeham, Y. Moolani, J. Silvester, A. Y. Ten, W. Bakker, K. Tsuchihara, S. L. Berger, R. P. Hill, R. G. Jones, M. Tsao, M. O. Robinson, C. B. Thompson, G. Pan and T. W. Mak, *Genes Dev.*, 2011, **25**, 1041–51.
15 S. M. Ceccarelli, O. Chomienne, M. Gubler and A. Arduini, *J. Med. Chem.*, 2011, **54**, 3109–3152.
16 A. Bentebibel, D. Sebastián, L. Herrero, E. López-Viñas, D. Serra, G. Asins, A.

Paulino Gómez-Puertas, Fausto G. Hegardt, P. Gómez-Puertas and F. G. Hegardt, *Biochemistry*, 2006, **45**, 4339–4350.
17 P. Mera, A. Bentebibel, E. López-Viñas, A. G. Cordente, C. Gurunathan, D. Sebastián, I. Vázquez, L. Herrero, X. Ariza, P. Gómez-Puertas, G. Asins, D. Serra, J. García and F. G. Hegardt, *Biochem. Pharmacol.*, 2009, **77**, 1084–1095.
18 W. A. Heggermont, A.-P. Papageorgiou, S. Heymans and M. van Bilsen, *Eur. J. Heart Fail.*, 2016, **18**, 1420–1429.
19 K. Makowski, P. Mera, J. Ariza, D. Serra, J. Garcia, L. Herrero, M. López and A. Venegas, *Rev. Bionatura*, 2019, **4**, 1–5.
20 A. Gautier and M. J. Hinner, *Site-Specific Protein Labeling Methods Protoc.*, 2015, 1–267.
21 M. C. Cheng, X. H. Qiang and C. M. Du, *Chinese Sci. Bull.*, 2013, **58**, 1256–1261.
22 C. Wang, Q. Chen, Z. Wang and X. Zhang, *Angew. Chemie - Int. Ed.*, 2010, **49**, 8612–8615.
23 H. Cabral, K. Miyata, K. Osada and K. Kataoka, *Chem. Rev.*, 2018, **118**, 6844–6892.
24 A. Harada and K. Kataoka, *Polym. J.*, 2018, **50**, 95–100.
25 S. Quader and K. Kataoka, *Mol. Ther.*, 2017, **25**, 1501–1513.
26 J. Garcia-Chica, W. K. D. Paraiso, S. Tanabe, D. Serra, L. Herrero, N. Casals, J. Garcia, X. Ariza, S. Quader and R. Rodriguez-Rodriguez, *Nanomedicine (Lond).*, 2020, **15**, 1617–1636.
27 H. Uchida, K. Miyata, M. Oba, T. Ishii, T. Suma, K. Itaka, N. Nishiyama and K. Kataoka, *J. Am. Chem. Soc.*, 2011, **133**, 15524–15532.
28 H. Uchida, K. Itaka, T. Nomoto, T. Ishii, T. Suma, M. Ikegami, K. Miyata, M. Oba, N. Nishiyama and K. Kataoka, *J. Am. Chem. Soc.*, 2014, **136**, 12396–12405.
29 C. Y. Lin, F. Perche, M. Ikegami, S. Uchida, K. Kataoka and K. Itaka, *J. Control. Release*, 2016, **235**, 268–275.
30 S. T. Crowley, Y. Fukushima, S. Uchida, K. Kataoka and K. Itaka, *Mol. Ther. - Nucleic Acids*, 2019, **17**, 465–476.
31 Y. Ma, S. M. Temkin, A. M. Hawkridge, C. Guo, W. Wang, X. Y. Wang and X. Fang, *Fatty acid oxidation: An emerging facet of metabolic transformation in cancer*, Elsevier B.V., 2018, vol. 435.
32 L. S. Pike, A. L. Smift, N. J. Croteau, D. A. Ferrick and M. Wu, *Biochim. Biophys. Acta - Bioenerg.*, 2011, **1807**, 726–734.
33 M. Allen, M. Bjerke, H. Edlund, S. Nelander and B. Westermark, *Sci. Transl. Med.*, 2016, **8**, 354re3-354re3.
34 S. Kant, P. Kesarwani, A. Prabhu, S. F. Graham, K. L. Buelow, I. Nakano and P. Chinnaiyan, *Cell Death Dis.*, 2020, **11**, 1–13.
35 B. Juraszek, J. Czarnecka-Herok and K. A. Nałęcz, *J. Neurochem.*, 2020, jnc.15124.
36 A. S. Divakaruni, W. Y. Hsieh, L. Minarrieta, T. N. Duong, K. K. O. Kim, B. R. Desousa, A. Y. Andreyev, C. E. Bowman, K. Caradonna, B. P. Dranka, D. A. Ferrick, M. Liesa, L. Stiles, G. W. Rogers, D. Braas, T. P. Ciaraldi, M. J. Wolfgang, T. Sparwasser, L. Berod, S. J. Bensinger and A. N. Murphy, *Cell Metab.*, 2018, **28**, 490-503.e7.
37 Z. Liposits, I. Merchenthaler, W. C. Wetsel, J. J. Reid, P. L. Mellon, R. I. Weiner and A. Negro-Vilar, *Endocrinology*, 1991, **129**, 1575–1583.
38 B. Taïb, K. Bouyakdan, C. Hryhorczuk, D. Rodaros, S. Fulton and T. Alquier, *J. Biol. Chem.*, 2013, **288**, 37216–37229.
39 A. C. Hunter, *Adv. Drug Deliv. Rev.*, 2006, 58, 1523–1531.
40 J. Sperry, M. C. Condro, L. Guo, D. Braas, N. Vanderveer-Harris, K. K. O. Kim, W. B. Pope, A. S. Divakaruni, A. Lai, H. Christofk, M. G. Castro, P. R. Lowenstein, J. E.

Le Belle and H. I. Kornblum, *iScience*, 2020, **23**, 101453.
41 S. J. Choi, F. Kim, M. W. Schwartz and B. E. Wisse, *Am. J. Physiol. Metab.*, 2010, **298**, E1122–E1130.
42 J. F. Mir, S. Zagmutt, M. P. Lichtenstein, J. García-Villoria, M. Weber, A. Gracia, G. Fabriàs, J. Casas, M. López, N. Casals, A. Ribes, C. Suñol, L. Herrero and D. Serra, *Mol. Neurobiol.*, 2018, **55**, 7216–7228.
43 H. Lin, S. Patel, V. S. Affeck, I. Wilson, D. M. Turnbull, A. R. Joshi, R. Maxwell, E. A. Stoll, V. S. Affleck, I. Wilson, D. M. Turnbull, A. R. Joshi, R. Maxwell and E. A. Stoll, *Neuro. Oncol.*, 2017, **19**, 43–54.
44 L. Mo, L. Hou, D. Guo, X. Xiao, P. Mao and X. Yang, *Int. J. Pharm.*, 2012, **436**, 815–824.
45 J. M. Rabanel, P. A. Piec, S. Landri, S. A. Patten and C. Ramassamy, *J. Control. Release*, 2020, **328**, 679–695.
46 R. Vadivelu, H. Kamble, M. Shiddiky and N.-T. Nguyen, *Micromachines*, 2017, **8**, 94.
47 A. Tchoryk, V. Taresco, R. H. Argent, M. Ashford, P. R. Gellert, S. Stolnik, A. Grabowska and M. C. Garnett, *Bioconjug. Chem.*, 2019, **30**, 1371–1384.
48 K. Kataoka, T. Matsumoto, M. Yokoyama, T. Okano, Y. Sakurai, S. Fukushima, K. Okamoto and G. S. Kwon, *J. Control. Release*, 2000, **64**, 143–153.
49 New England Biolabs Inc., Reaction Conditions for Chemical Coupling with CoA-SH (S9352S), https://international.neb.com/protocols/2012/08/09/reaction-conditions-for-chemical-coupling-with-coa-sh-s9352s, (accessed 11 May 2020).
50 M. I. Malandrino, R. Fucho, M. Weber, M. Calderon-Dominguez, J. F. Mir, L. Valcarcel, X. Escoté, M. Gómez-Serrano, B. Peral, L. Salvadó, S. Fernández-Veledo, N. Casals, M. Vázquez-Carrera, F. Villarroya, J. J. Vendrell, D. Serra and L. Herrero, *Am. J. Physiol. - Endocrinol. Metab.*, 2015, **308**, E756–E769.